PAPER

Stability of MAPbI₃ perovskite grown on planar and mesoporous electron-selective contact by inverse temperature crystallization†

Ramya Krishna Battula, [ID]abc Ganapathy Veerappan,a P. Bhyrappa, [ID]b C. Sudakar [ID]c and Easwaramoorthi Ramasamy [ID]*a

Single crystalline perovskite solar cells (PSC) are promising for their inherent stability due to the absence of grain boundaries. While the development of single crystals of perovskite with enhanced optoelectronic properties is known, studies on the growth, device performance and understanding of the intrinsic stability of single crystalline perovskite thin film solar cell devices fabricated on electron selective contacts are scarcely explored. In this work, we examine the impact of mesoporous TiO_2 (m-TiO_2) and planar TiO_2 (p-TiO_2) on the growth of single crystalline-methyl ammonium lead iodide (SC-MAPbI₃) film, PSC device performance and film stability under harsh weather conditions (T ~ 85 °C and RH ~ 85%). Self-grown SC-MAPbI₃ films are developed on m-TiO_2 and p-TiO_2 by inverse temperature crystallization under ambient conditions without the need for sophisticated glove-box processing. The best device with m-TiO_2 as an electron transport layer showed a promising power conversion efficiency of 3.2% on an active area of 0.3 cm² in hole transport material free configuration, whereas, only 0.7% was achieved for the films developed on p-TiO_2. Complete conversion of precursor to perovskite phase and better surface coverage of the film leading to enhanced absorption and reduced defects of single crystalline perovskite on m-TiO_2 compared to its p-TiO_2 leads to this large difference in efficiency. Mesoporous device retained more than 70% of its initial performance when stored at 30 °C under dark for more than 5000 h at 50% RH; while the planar device degraded after 1500 h. Thermal and moisture endurance of SC-MAPbI₃ films are investigated by subjecting them to temperatures ranging from 35 °C to 85 °C at a constant relative humidity (RH) of 85%. X-ray diffraction studies show that the SC-MAPbI₃ films are stable even at 85 °C and 85% RH, with only slight detection (30–35%) of PbI_2 at these conditions. This study highlights the superior stability of SC-MAPbI₃ films which paves way for further studies on improving the stability and performance of the ambient processed PSCs.

Introduction

Organic–inorganic hybrid perovskites with a molecular formula of ABX₃ (A = MA, FA, B = Pb, Sn, X = I, Br, Cl) have received significant attention since their first successful application as an absorber material in solar cells with 3.8% power conversion efficiency (PCE).[1] Subsequent developments in perovskite composition, carrier selective contacts and device fabrication processes led to rapid progress in PCE exceeding 25% in laboratory scale perovskite solar cells (PSC), raising its commercial viability.[2] Stability of PSCs under real-time environmental conditions (*i.e.*, moisture, oxygen, temperature and light) is one of the critical issues that needs to be addressed for considering this technology as a serious contender to rival the existing wafer and thin-film based photovoltaics. The stability of PSC is mainly affected by intrinsic degradation of perovskite absorber material and its interfaces with electron and hole selective contacts. When exposed to moisture, perovskite reacts with water molecules and hydrolyzes back to its precursors *via* multiple pathways.[3] This gives rise to structural, optical and morphological changes and subsequent deterioration of photovoltaic performance. The perovskite research community has devised various strategies to improve the stability of PSCs. For example, incorporating different combinations of cations and anions, judicial selection of electron selective contacts, and introducing hydrophobic passivation layer on perovskite absorber are found to improve the operational stability of PSC.[4]

High efficiency PSC are usually prepared by spin deposition of precursor solution on carrier selective contact coated

ᵃCentre for Solar Energy Materials, International Advanced Research Centre for Powder Metallurgy and New Materials (ARCI), Hyderabad 500005, India. E-mail: easwar@arci.res.in

ᵇDepartment of Chemistry, Indian Institute of Technology Madras, Chennai 600036, India

ᶜMultifunctional Materials Lab, Department of Physics, Indian Institute of Technology Madras, Chennai 600036, India

† Electronic supplementary information (ESI) available. See DOI: 10.1039/d0ra05590e

transparent conductive oxide substrates followed by annealing at 100 °C. Large number of grain boundaries in the resultant polycrystalline perovskite film act as active sites for moisture ingress into the grain.[3,5,6] This is due to the amorphous and non-stoichiometric nature of the inter-granular layer that allows rapid diffusion of moisture into the perovskite film. The grain boundaries also act as recombination sites for charge carriers, resulting in lower diffusion lengths, shorter carrier lifetime, and fast ion migration leading to performance losses. Hence, minimizing the grain boundaries and increasing the grain size has emerged as a viable route to improve the stability and performance of PSC.[7]

Single-crystalline (SC) perovskite has potential to address most of the afore mentioned shortcomings due to the absence of grain boundaries.[8–10] Other benefits of SC perovskite include high electron diffusion lengths exceeding 175 μm and trap densities at least 5 times lower than their polycrystalline counterparts.[8] Solution grown free-standing SC perovskites are successfully used for studying the fundamental properties. However, fabrication of working device is not straightforward due to difficulties in integrating SC perovskite into device architecture, a weak interface between the SC perovskite and carrier selective contacts, thickness of the crystal being higher than the diffusion length to name a few.[11] Hence, the development of SC perovskite on the desired substrate is of great importance to exploit the merits of SC perovskites in photovoltaics. Perovskite has a unique property of crystallizing from precursor solution at high temperature which is inverse of the conventional crystallization. These characteristics have led to the development of standalone perovskite single crystals and films by inverse temperature crystallization (ITC). This methodology in a confined space is the most feasible method due to its ease of processing, faster growth rate, flexibility in the choice of the substrates, and controllable film thickness.[12] Chen et. al.[13] have grown uniform SC perovskite films on a range of flat substrates including silicon wafer, polyethylene terephthalate, HOPG and ITO by ITC method. Zhao et. al.[14] have reported the growth of SC-MAPbI$_3$ film on FTO substrate by ITC method and obtained PCE of 8.7% on devices with an active area of 0.01 cm^2. The highest PCE for single crystalline PSCs of 21.09% was reported by Chen et. al.[15] using ITO/poly(triarylamine) (PTAA)/MAPbI$_3$/C$_{60}$/bathocuproine (BCP)/copper (Cu) architecture.

The electron selective contact plays a critical role in the performance and stability of PSC, however, its exact effect on PCE is under debate for a long time. Abate and Gagliardi studied the influence of material and morphology of electron selective contact on the stability of polycrystalline PSC and evidently shown that mesoporous electron selective contact enables PSC more resilient to ion defect migration.[16] Despite reports of SC perovskites grown directly over the device grade substrates, not much emphasis has been laid on the influence of carrier selective contact on the growth, performance, and stability of the single crystalline perovskites.

In this work, methylammonium lead iodide (MAPbI$_3$) perovskite single crystals are directly grown on planar and mesoporous TiO$_2$ electron selective contacts coated FTO glass substrate by ITC method. Structural analysis and device characteristics indicate enhanced crystalline feature and photovoltaic performance of MAPbI$_3$ grown on mesoporous TiO$_2$. Accelerated aging tests carried out at elevated temperature and high humidity confirms the robustness of the perovskite films grown on electron selective contact by ITC.

Experimental

Materials

TiO$_2$ powders with a particle size of 20 nm were purchased from Dynamo. Other chemicals such as titaniumbis(acetylacetonate) di-isopropoxide (Ti(acac)$_2$(OiPr)$_2$) (75 wt.% in isopropanol), hydroiodic acid (HI, 57 wt% in H$_2$O), hydrochloric acid (HCl, 37 wt.% in H$_2$O), diethyl ether (DEE, ≥99.0%), lead iodide, (PbI$_2$, 99%), 2-propanol (IPA, ≥98%), N,N′-dimethylformamide (DMF, 99.8%) and 1-butanol (99.8%) were purchased from Sigma-Aldrich. Methylamine (40% in methanol) and γ-butyrolactone (GBL, ˃99%) were purchased from TCI Chemicals. All the chemicals purchased were used without any further purification or processing.

Planar and mesoporous TiO$_2$ carrier selective contacts

The FTO (sheet resistance of 8 Ω sq^{-1}) glass substrates were patterned using zinc dust and 2 M HCl. The substrates are cut and cleaned for 10 minutes each time in an aqueous soap solution, DI water, acetone and IPA. The planar TiO$_2$ (p-TiO$_2$) layer was deposited by spin coating 0.15 M and 0.3 M Ti(acac)$_2$(OiPr)$_2$ in 1-butanol at 4000 rpm for 20 s to get ~80 nm film. The mesoporous (m-TiO$_2$) layer is deposited on the p-TiO$_2$ layer by spin coating the TiO$_2$ paste diluted in ethanol at 3000 rpm for 30 s to get ~500 nm layer. The substrates are finally treated with 40 mM aqueous TiCl$_4$ solution at 100 °C for 1 h and rinsed with DI water. The substrates are annealed at 500 °C for 30 min at 5 °C min^{-1} ramping rate after each layer.

Synthesis of MAPbI$_3$ by ITC method

Methylammonium iodide (MAI) is synthesized, according to the process reported in the literature.[17] MAI and PbI$_2$ is dissolved in GBL to obtain 1.23 M solution. This solution is filtered using 450 nm pore size polytetrafluoroethylene (PTFE) membrane. Two TiO$_2$ electrodes are kept separated at a distance of 20 μm by placing a spacer between the electrodes. This set up is clamped, vertically dipped into the solution and kept on a hotplate at 110 °C as schematically shown in Fig. 1. Due to the thin, uniform gap, the solution moves upwards by capillary action. Further, the temperature gradient between the top and bottom end of the substrate aids in crystallization. After 18 h, (Fig. S1†), the substrates are removed from the solution, carefully separated, washed with DEE and annealed at 110 °C for 20 min. The entire fabrication is carried out in ambient conditions (~35 °C and 50% RH, Hyderabad, India) eliminating the need for sophisticated glove-box processing. It has been observed that the MAPbI$_3$ films grown on p-TiO$_2$ are non-uniform and transparent. By contrast, the films grown on m-TiO$_2$ are denser with complete surface coverage of underneath TiO$_2$ layer, as shown in Fig. 1.
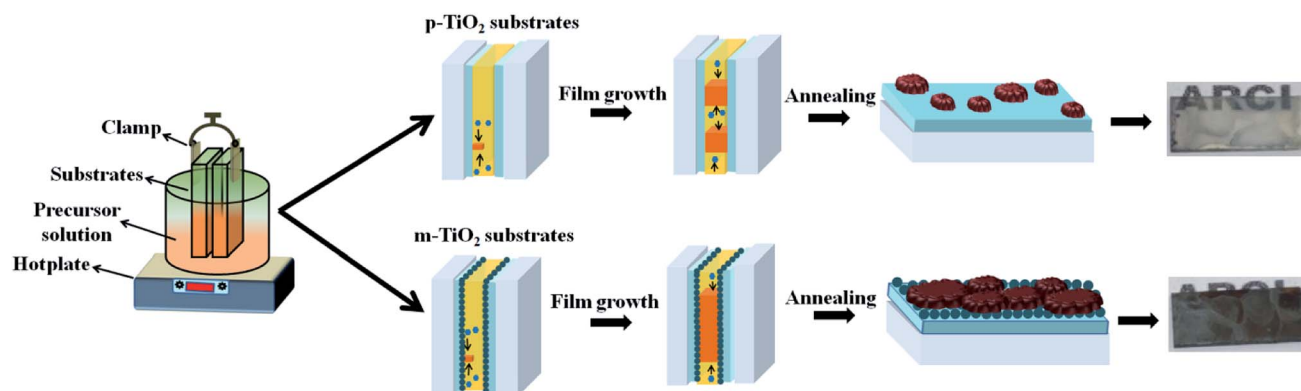
Fig. 1 Schematic diagram describes the growth of MAPbI$_3$ perovskite on planar (top) and mesoporous TiO$_2$ electron-selective contact coated FTO glass substrates (bottom) by ITC.

Characterization and stability studies

The surface morphology is examined using field emission scanning electron microscope (FE-SEM, ZEISS GeminiSEM 500). Transmission electron microscopy (TEM) studies are carried out using TecnaiG2 (FEI) machine operating at 200 kV acceleration voltage. XRD patterns are obtained by X-ray diffractometer (D8 Advance, Bruker). RMS roughness measurement is carried out using stylus profilometer (DektakXT, Bruker) with 50 nm stylus radius. The steady state photoluminescence (PL) studies were carried out using an FL-1039A/40A, Horiba Instruments spectrofluorometer. UV-vis absorption spectra of the MAPbI$_3$ thin-films were recorded on a Cary 5000 spectrophotometer. The current–voltage (I–V) characteristics are measured using Newport Oriel solar simulator equipped with a Xenon lamp and a Keithley source meter. The incident light intensity is calibrated to one Sun illumination using an NREL certified silicon photodiode. The moisture and temperature-controlled tests are carried out in an environmental chamber WK-3-180/70 Weiss

GmBH. In order to study their moisture and temperature endurance, the films were subjected to controlled temperature and humidity conditions in an environmental chamber for 6 h each at 35 °C, 60 °C and 85 °C at a constant RH of 85%. The temperature and RH test parameters were chosen according to the ISOS (International Summit on Organic photovoltaic Stability) D-3 damp heat test.

Results and discussion

Growth of MAPbI$_3$ on planar and mesoporous TiO$_2$ electron selective contacts

Fig. 2 depicts the surface morphology of the TiO$_2$ and the MAPbI$_3$ films grown on both planar and mesoporous templates. Fig. 2(a) reveals the perfect coverage of the underneath FTO grains with the planar TiO$_2$ blocking layer. Fig. 2(b) shows the haphazard distribution of the single crystals of MAPbI$_3$ greater than 10 μm size over the p-TiO$_2$ layer. It can be observed from
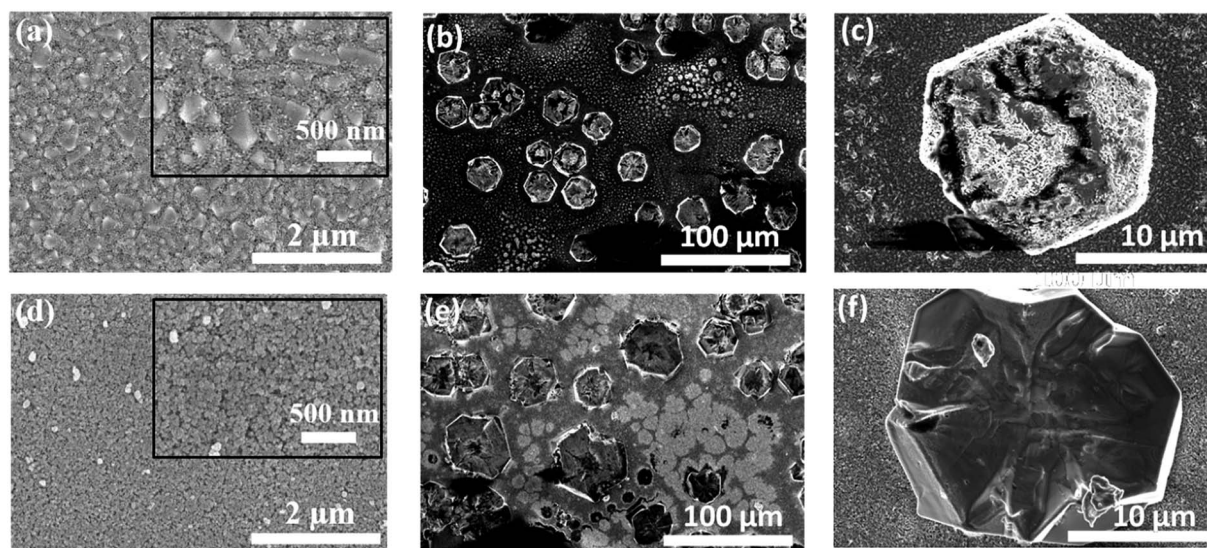

Fig. 2 FE–SEM images of (a) planar TiO$_2$ and (d) mesoporous TiO$_2$ coated FTO substrate (insets show the high magnification images). Low and high magnification FE–SEM images of MAPbI$_3$ coated on planar (b and c) and mesoporous TiO$_2$ templates (e and f).
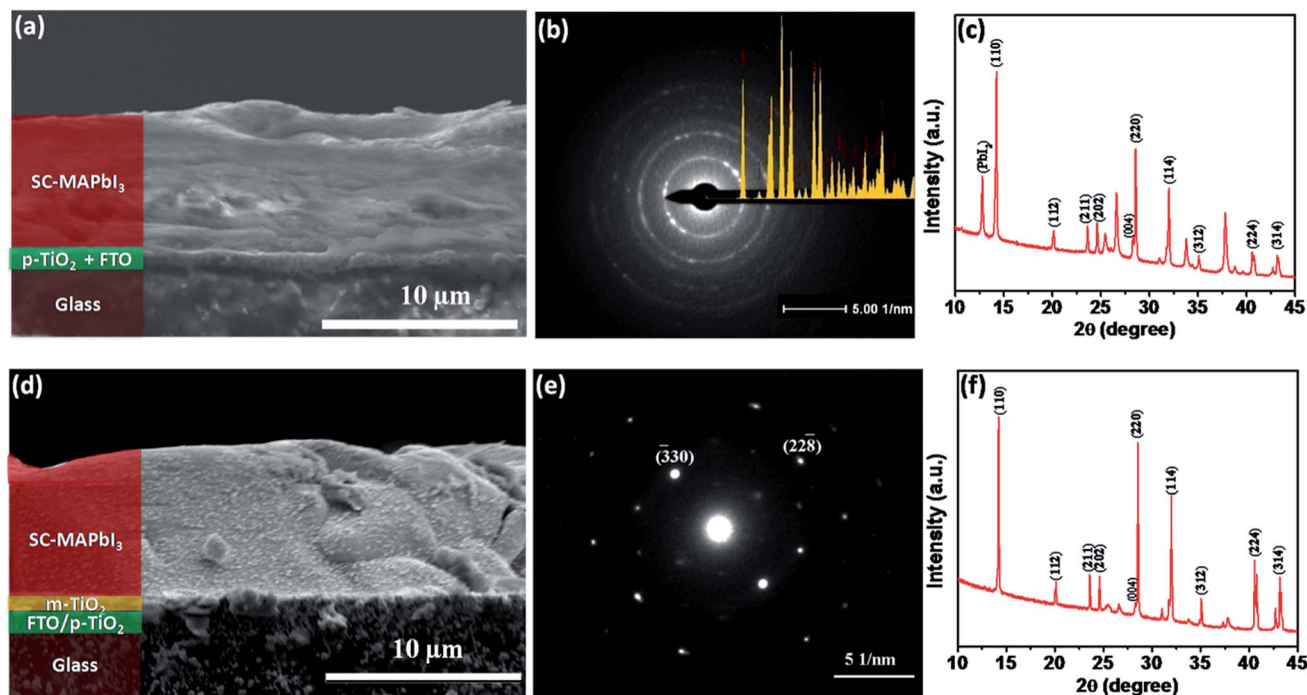
Fig. 3 (a and d) Cross-sectional FE-SEM images, (b and e) SAED patterns, and (c and f) X-ray diffraction pattern of MAPbI$_3$ perovskite on planar TiO$_2$ (a–c) and on mesoporous TiO$_2$ (d–f) electron selective contact.

the high magnification image shown in Fig. 2(c) that the crystals are hexagonal in shape with tiny crystallites residing on them. These tiny crystallites are mainly originating due to the unconverted precursors.[18] The inference for this is also supported by the XRD patterns (Fig. 3(c)) as discussed in detail in the following paragraph. Fig. 2(d) shows the surface morphology of the m-TiO$_2$ film with spherical shaped mesoporous particles evenly distributed all over the p-TiO$_2$ film. The MAPbI$_3$ film grown on this substrate, shown in Fig. 2(e), also has similar morphological features as observed in Fig. 2(b) with crystals sparsely populated on the m-TiO$_2$ film but with each of these crystals grown with smoother surface (Fig. S2†) and larger size as clearly seen in Fig. 2(f). This is mainly due to the

complete conversion of the precursors owing to slow crystallization and coherent growth of large number of nucleation sites available on the m-TiO$_2$ surface compared to the fast crystallization resulting in incomplete conversion on the flat p-TiO$_2$.[19,20]

Fig. 3(a) shows the cross-sectional image of the MAPbI$_3$/p-TiO$_2$. The film is rough with unclear interface between the p-TiO$_2$ and the MAPbI$_3$ film. The selected area electron diffraction (SAED) pattern is shown in Fig. 3(b) taken from a representative crystal (not shown) indicates the polycrystalline nature. The presence of unconverted precursors which is clearly discerned from the XRD pattern shown in Fig. 3(c) could result into polycrystalline nature. Fig. 3(d) shows the cross-sectional FE-SEM image of the MAPbI$_3$ film that clearly depicts a sharp
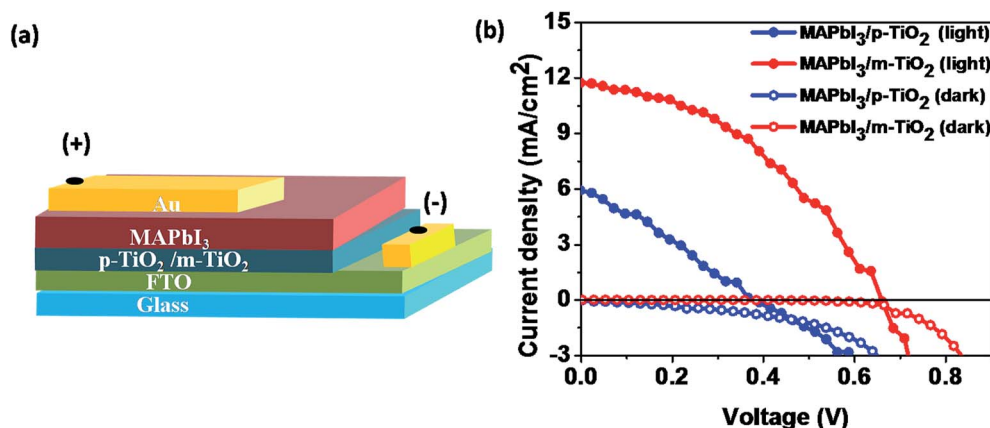

Fig. 4 (a) Device schematic and (b) current–voltage characteristics (forward scan) of HTM-free MAPbI$_3$ perovskite solar cells prepared on planar and mesoporous-TiO$_2$ electron selective contacts.
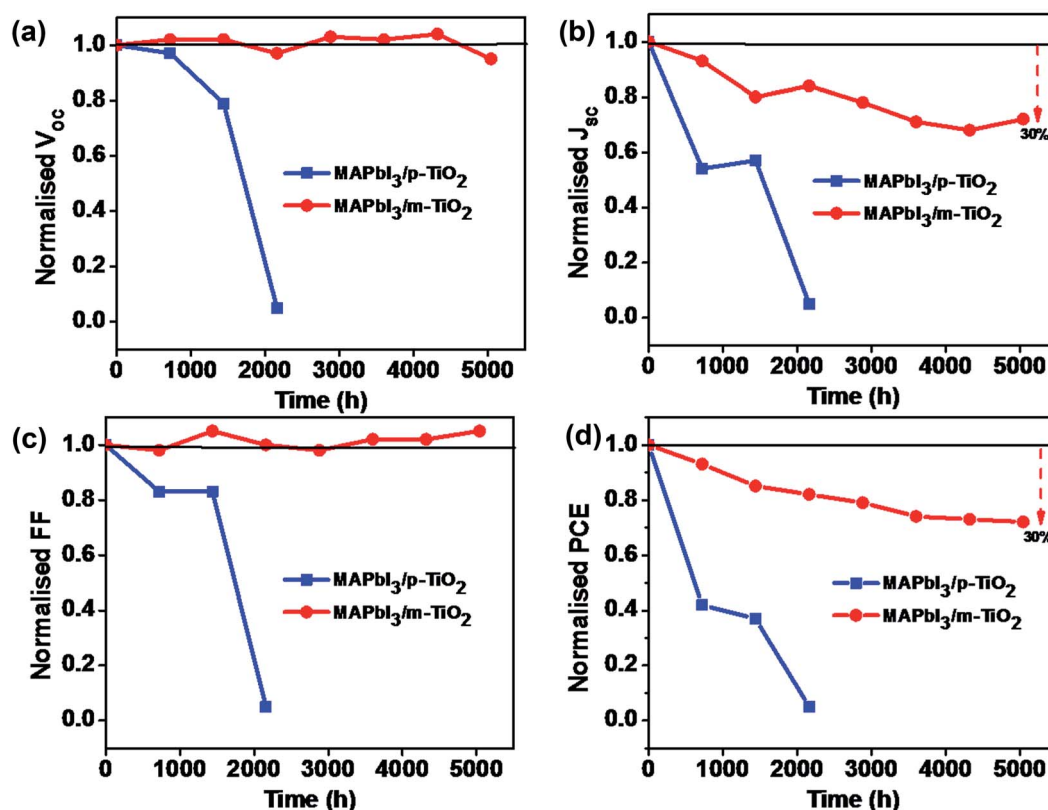
Fig. 5 Evolution of device parameters of HTM-free MAPbI$_3$ perovskite solar cells prepared on planar and mesoporous-TiO$_2$ electron selective contacts:(a) open-circuit voltage, V_{OC}, (b) short-circuit current density, J_{SC}, (c) fill factor, FF and (d) power conversion efficiency, PCE. Devices were aged under ambient conditions (50% RH, 30 °C) and photovoltaic performances are carried out at regular interval under one Sun conditions.

interface between the MAPbI$_3$ film and the m-TiO$_2$ surface. The interface quality is very crucial in deciding the charge transfer properties and proper functioning of the device. SAED pattern acquired from the single crystals grown on m-TiO$_2$ show spot pattern. Fig. 3(e) shows one such ED pattern with zone axis of [221]. Using simulated ED pattern the single crystal pattern is generated which matches with the proposed zone axis (Fig. S3†). Thus, ITC process on m-TiO$_2$ leads to the growth of single crystals populated on the film. The XRD pattern of these films reveal tetragonal phase is in agreement with the previously reported literature as depicted in Fig. 3(f).[14] The sharp cleavage of the (004) and (220) planes indicates the high crystallinity and tetragonal phase of the films.[21] The relative intensities in both

films further suggest that the single crystals grown on TiO$_2$ have wide distribution in orientation w.r.t. the direction perpendicular to the substrate surface.

Photovoltaic performance

The device configuration employed to evaluate the photovoltaic performance of SC-MAPbI$_3$ perovskite based solar cell is schematically shown in Fig. 4(a). Solution deposition of hole transporting material (HTM) usually weakens perovskite–substrate interface and therefore HTM-free configuration is adopted in the present study. Device fabrication was completed by thermal evaporation of 80 nm thick Au cathode on SC-MAPbI$_3$. Fig. 4(b)

Table 1 Photovoltaic performance of HTM-free MAPbI$_3$PSC prepared on planar and mesoporous TiO$_2$ electron selective contacts

Device ID	Duration (h)	V_{OC} (V)	J_{SC} (mA.cm^{-2})	FF	PCE (%)	Retention in PCE (%)
MAPbI$_3$/p-TiO$_2$	0	0.38	5.96	0.29	0.7	100
	1500	0.30	3.43	0.24	0.2	~30
	5000	—	—	—	—	0
MAPbI$_3$/m-TiO$_2$	0	0.66	11.72	0.41	3.2	100
	1500	0.67	9.35	0.43	2.6	~80
	5000	0.63	8.47	0.43	2.2	~70

compares the dark and illuminated current–voltage characteristics of PSCs. The MAPbI$_3$ perovskite prepared on planar-TiO$_2$ (labeled as MAPbI$_3$/p-TiO$_2$) shows a fill factor (FF) of only 0.29 indicating poor quality of diode characteristics. The open-circuit voltage (V_{OC}) of 380 mV and short-circuit current density (J_{SC}) of 5.96 mA cm^{-2}are also significantly lower than the values reported in the literature. Uncovered area in MAPbI$_3$/p-TiO$_2$ electrode might have led to shunting of Au cathode and adversely affecting the junction quality. SC-MAPbI$_3$ prepared on a mesoporous-TiO$_2$ (labeled as MAPbI$_3$/m-TiO$_2$) has high V_{OC} (660 mV) and J_{SC} (11.72 mA cm^{-2}) leading to a power conversion efficiency of 3.2%. The improved FF (0.41) is attributed to the presence of m-TiO$_2$ layer which prevents the direct contact between the FTO substrate and Au cathode and improved junction quality. The superior J_{SC} agrees with enhanced surface coverage and optical absorption of MAPbI$_3$/m-TiO$_2$ as shown in Fig. 2(e) and S4,† respectively.

Fig. 5 shows the evolution of device parameters of HTM-free MAPbI$_3$ perovskite solar cells prepared on planar and mesoporous-TiO$_2$ electron selective contacts when aged at 30 °C and 50% RH. Table 1 quantifies the photovoltaic parameters of the fresh and aged devices. The planar device retained only 35% of its PCE when aged for 1500 h. This decrease in efficiency is due to the decreased absorbance and morphological transformation that happens over time (refer Fig. S4 and S5(a) in ESI†), respectively. The mesoporous device retained more than 70% of its PCE even after 5000 h of aging, which is the highest reported stability amongst SC-MAPbI$_3$ solar cells to the best of our knowledge.[22,23] Further trapping of charges will be minimized due to this micro-structural improvement. Negligible changes could be observed in V_{OC} and FF of the mesoporous devices as shown in Fig. 5(a) and (c). However, gradual drop over time in J_{SC} as shown in Fig. 5(b) led to the drop in PCE. This can only be attributed to the drop-in absorbance of the film as shown in Fig. S4† which eventually affects carrier generation resulting in low current density. It is worthwhile to mention here that similar aging tests carried out on MAPbI$_3$ film on both planar and mesoporous templates did not show any notable structural changes as observed from X-ray diffraction (Fig. S6†). However, MAPbI$_3$ film grown on mesoporous TiO$_2$ exhibits higher PL intensity (Fig. S7†) than that of MAPbI$_3$ grown on planar TiO$_2$. Based on the relevant literatures[23–25] and considering similar perovskite precursor and experimental conditions, the enhanced PL intensity is plausibly attributed to reduced trap densities.

Stability under accelerated aging condition

Even after 5000 h of aging at 30 °C and 50% RH, the MAPbI$_3$/m-TiO$_2$ did not show any trace of PbI$_2$ or significant morphological breakdown as recorded by the XRD pattern and FE-SEM images (refer Fig. S6(b) and S5(b) in ESI†). Only indication of degradation was inferred from a slight drop in absorbance observed as shown in Fig. S4.† This inbuilt tolerance of MAPbI$_3$/m-TiO$_2$ film after 5000 h in mild conditions has motivated us to study its behavior under extreme stressing conditions, i.e. exposing the films at higher temperature and relative humidity

conditions. For this purpose, the films were subjected to 3 different temperatures of 35 °C, 60 °C and 85 °C at a constant RH of 85% for 6 h each under ambient air flow. For comparison, the behavior of MAPbI$_3$/p-TiO$_2$ was also recorded under similar conditions.

The surface morphology and optical characterization by FE-SEM and UV-Vis spectrophotometer were carried out on the films subjected to the extreme stressing conditions and their corresponding results are summarized in Fig. 6(a–h), (i and j), respectively. The fresh MAPbI$_3$/p-TiO$_2$ shown in Fig. 6(a) is made up of tiny crystallites on its surface in contrary to the smooth morphology of its mesoporous counterpart (Fig. 6(e)). From Fig. 6(a–h) it can be clearly seen that the crystal morphology is deteriorating under increased exposure to stressing conditions in both planar and mesoporous cases. This could be because of the inclination of the perovskite crystal edges to form hydrogen bonding between the incoming water molecules and the perovskite lattice resulting in morphological changes.[26] Also, the intercalation of moisture into the perovskite structure is only the first stage of degradation before it converts into the intermediate hydrate or dihydrate forms of MAPbI$_3$. The formation of these intermediate stages could not be identified structurally up to the aging temperatures of 60 °C, however, this has resulted in a loss in absorbance as seen in Fig. 6(i and j).[27] At 85 °C, the morphology of the MAPbI$_3$ in both the cases has completely collapsed to a rod-like structure as shown in Fig. 6(d and h). This indicates that degradation leading to PbI$_2$ under these extreme stressing conditions gets initiated noticeably. XRD pattern obtained at different aging temperatures detailed in the following paragraph also supports these facts (Fig. 7(b)).[28]

The lower absorbance of the fresh film in Fig. 6(i) can be attributed to the transparent film quality as can be seen in its photographic image shown in Fig. 1. However, freshly grown SC-MAPbI$_3$/m-TiO$_2$ showed better absorbance compared to the MAPbI$_3$/p-TiO$_2$ films in the 500 to 750 nm range, as shown in Fig. 6(j). The superior absorbance is due to the large number of nucleation sites available for slow crystallization and dense crystal growth on the mesoporous substrate compared to the planar substrate.

To check for the presence of PbI$_2$, which is the most commonly identified product on degradation of MAPbI$_3$, XRD characterization was done on the fresh and aged films, and its corresponding patterns are given in Fig. 7. In Fig. 7(a), freshly grown MAPbI$_3$/p-TiO$_2$ film showed a small peak of unconverted PbI$_2$ at 12.6° corresponding to (001) plane[21] apart from the MAPbI$_3$ peaks indicating that the fresh film itself did not crystallize homogeneously. In Fig. 7(b), the MAPbI$_3$/m-TiO$_2$ fresh films showed intense peak at 14.1°,which is the characteristic reflection from (110) plane of MAPbI$_3$.[29–31] No trace of PbI$_2$ is found indicating full conversion of the reactants. As the films are exposed to the stressing environment, i.e., upon increasing the temperature to 35 °C and 60 °C at constant RH of 85%, the films in both cases showed minimal traces of degradation with only diminishing peak intensities of the perovskite phase. The early stage of degradation in perovskite phases which is mostly undetectable in XRD can be discerned from the absorbance
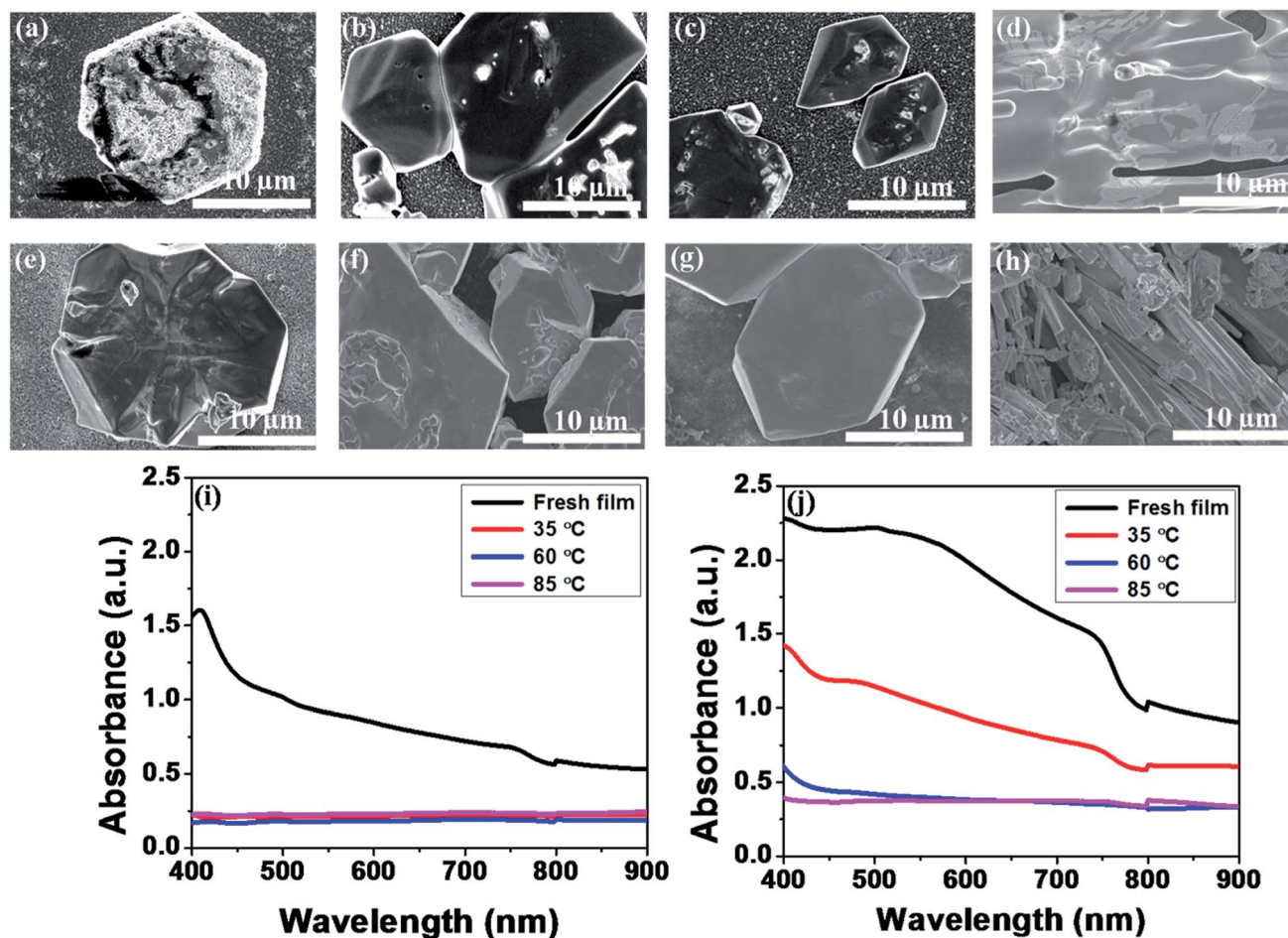
Fig. 6 FESEM images of (a and e) fresh films (as prepared in ambient conditions of 30 °C, 50% RH) and films aged by exposing to (b and f) 35 °C, (c and g) 60 °C and (d and h) 85 °C of MAPbI$_3$/p-TiO$_2$ (a–d) and MAPbI$_3$/m-TiO$_2$ (e–f), respectively. Optical absorption of the fresh and aged films of (i) MAPbI$_3$/p-TiO$_2$ and (j) MAPbI$_3$/m-TiO$_2$.

spectra and surface morphological changes observed from the SEM images as depicted in Fig. 6. At extreme conditions of exposures, *i.e.* temperature kept at 85 °C and humidity maintained at 85% RH, a small XRD peak of PbI$_2$ begins to show up

in the films fabricated on both planar and mesoporous TiO$_2$. These studies thus clearly bring out the quality of films and their endurance on the extreme temperature and humidity.
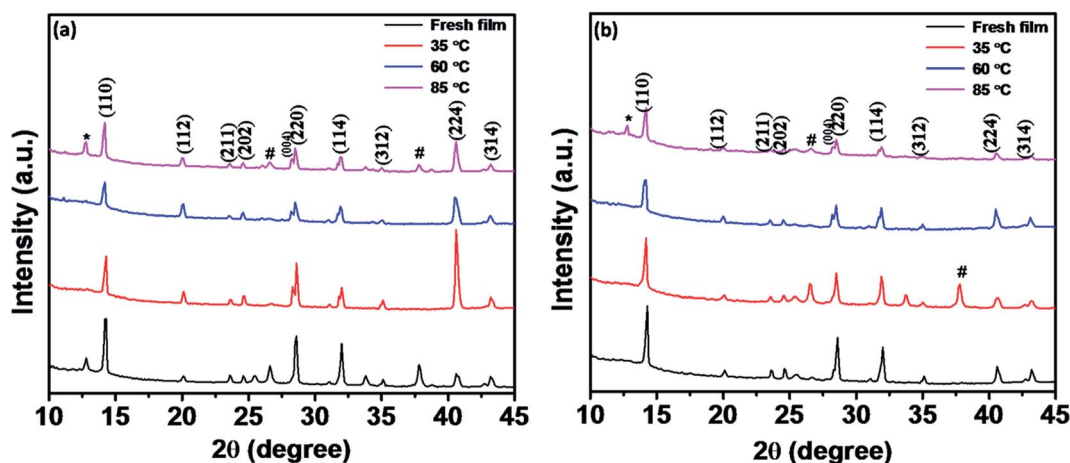

Fig. 7 XRD pattern of (a) MAPbI$_3$/p-TiO$_2$ and (b) MAPbI$_3$/m-TiO$_2$ treated at constant RH of 85% at 35 °C, 60 °C and 85 °C for 6 h each. * − PbI$_2$, # − FTO.

Conclusions

In summary, single crystalline perovskite films are successfully grown on planar and mesoporous TiO_2 substrates. Uniform and dense films grew on the mesoporous TiO_2 substrates compared to the planar TiO_2 electrodes due to the better interfacial area available for nucleation. The influence of the underneath TiO_2 layer on the device performance and stability is found to be very crucial. The SC-MAPbI$_3$ film developed on m-TiO_2 without a hole transporting material exhibited a promising efficiency of 3.2% on an active area of 0.3 cm^2, whereas a PCE of 0.7% is obtained for the planar device. Moreover, the mesoporous devices are found to be more stable than the planar devices, with 70% retention of their initial PCEs for more than 5000 h. This can be owed to the resilience of the mesoporous architecture towards performance losses arising from ion vacancy migration compared to the planar architecture. As there is no considerable degradation in the films in ambient conditions even after 5000 h of exposure, the effect of extreme temperature and humidity on SC-MAPbI$_3$ absorber material to degradation is investigated with respect to planar and mesoporous structure. It was observed that the films are stable even at 85 °C and 85% RH with only a slight detection of PbI_2. This establishes the robust nature of the single crystalline films. However, the mechanism of its degradation is yet to be completely understood as we could not find notable difference in the structural degradation with respect to the underneath TiO_2 layer when subjected to high stressing conditions. We conclude that the mesoporous template is the key for uniform growth, optimum device performance and stability of the SC-MAPbI$_3$ films. By carefully controlling the film growth parameters such as temperature, precursor concentration and surface roughness, better quality SC-MAPbI$_3$ films can be developed, which would further boost the performance.

Conflicts of interest

There are no conflicts to declare.

Acknowledgements

References

1 A. Kojima, K. Teshima, Y. Shirai and T. Miyasaka, *J. Am. Chem. Soc.*, 2009, **131**, 6050–6051.

2 *Best Research-Cell Efficiency Chart|Photovoltaic Research|NREL*, https://www.nrel.gov/pv/cell-efficiency.html, accessed 5 August 2019.

3 Q. Wang, B. Chen, Y. Liu, Y. Deng, Y. Bai, Q. Dong and J. Huang, *Energy Environ. Sci.*, 2017, **10**, 516–522.

4 N. Park, *Adv. Energy Mater.*, 2020, **10**, 1903106.

5 A. Gomez, S. Sanchez, M. Campoy-Quiles and A. Abate, *Nano Energy*, 2018, **45**, 94–100.

6 Q. Sun, P. Fassl, D. Becker-Koch, A. Bausch, B. Rivkin, S. Bai, P. E. Hopkinson, H. J. Snaith and Y. Vaynzof, *Adv. Energy Mater.*, 2017, **7**, 1700977.

7 X. Wang, W. Li, J. Liao and D. Kuang, *Sol. RRL*, 2019, **3**, 1800294.

8 Q. Dong, Y. Fang, Y. Shao, P. Mulligan, J. Qiu, L. Cao and J. Huang, *Science*, 2015, **347**, 967–970.

9 Y. Liu, Z. Yang, D. Cui, X. Ren, J. Sun, X. Liu, J. Zhang, Q. Wei, H. Fan, F. Yu, X. Zhang, C. Zhao and S. F. Liu, *Adv. Mater.*, 2015, **27**, 5176–5183.

10 D. Shi, V. Adinolfi, R. Comin, M. Yuan, E. Alarousu, A. Buin, Y. Chen, S. Hoogland, A. Rothenberger, K. Katsiev, Y. Losovyj, X. Zhang, P. A. Dowben, O. F. Mohammed, E. H. Sargent and O. M. Bakr, *Science*, 2015, **347**, 519–522.

11 H.-L. Yue, H.-H. Sung and F.-C. Chen, *Adv. Electron. Mater.*, 2018, **4**, 1700655.

12 R. Babu, L. Giribabu and S. P. Singh, *Cryst. Growth Des.*, 2018, **18**, 2645–2664.

13 Y.-X. Chen, Q.-Q. Ge, Y. Shi, J. Liu, D.-J. Xue, J.-Y. Ma, J. Ding, H.-J. Yan, J.-S. Hu and L.-J. Wan, *J. Am. Chem. Soc.*, 2016, **138**, 16196–16199.

14 J. Zhao, G. Kong, S. Chen, Q. Li, B. Huang, Z. Liu, X. San, Y. Wang, C. Wang, Y. Zhen, H. Wen, P. Gao and J. Li, *Sci. Bull.*, 2017, **62**, 1173–1176.

15 Z. Chen, B. Turedi, A. Y. Alsalloum, C. Yang, X. Zheng, I. Gereige, A. AlSaggaf, O. F. Mohammed and O. M. Bakr, *ACS Energy Lett*, 2019, **4**, 1258–1259.

16 A. Gagliardi and A. Abate, *ACS Energy Lett*, 2018, **3**, 163–169.

17 J.-H. Im, I.-H. Jang, N. Pellet, M. Grätzel and N.-G. Park, *Nat. Nanotechnol.*, 2014, **9**, 927–932.

18 J. Schlipf, A. M. Askar, F. Pantle, B. D. Wiltshire, A. Sura, P. Schneider, L. Huber, K. Shankar and P. Müller-Buschbaum, *Sci. Rep.*, 2018, **8**, 4906.

19 A. R. Pascoe, M. Yang, N. Kopidakis, K. Zhu, M. O. Reese, G. Rumbles, M. Fekete, N. W. Duffy and Y.-B. Cheng, *Nano Energy*, 2016, **22**, 439–452.

20 Y. Wu, A. Islam, X. Yang, C. Qin, J. Liu, K. Zhang, W. Peng and L. Han, *Energy Environ. Sci.*, 2014, **7**, 2934–2938.

21 Y. Fu, F. Meng, M. B. Rowley, B. J. Thompson, M. J. Shearer, D. Ma, R. J. Hamers, J. C. Wright and S. Jin, *J. Am. Chem. Soc.*, 2015, **137**, 5810–5818.

22 Y. Song, W. Bi, A. Wang, X. Liu, Y. Kang and Q. Dong, *Nat. Commun.*, 2020, **11**, 274.

23 Z. Chen, Q. Dong, Y. Liu, C. Bao, Y. Fang, Y. Lin, S. Tang, Q. Wang, X. Xiao, Y. Bai, Y. Deng and J. Huang, *Nat. Commun.*, 2017, **8**, 1890.

24 J. Jiang, Z. Jin, F. Gao, J. Sun, Q. Wang and S. F. Liu, *Adv. Sci.*, 2018, **5**, 1800474.

25 G. Han, T. M. Koh, S. S. Lim, T. W. Goh, X. Guo, S. W. Leow, R. Begum, T. C. Sum, N. Mathews and S. Mhaisalkar, *ACS Appl. Mater. Interfaces*, 2017, **9**, 21292–21297.

26 Z. Zhu, V. G. Hadjiev, Y. Rong, R. Guo, B. Cao, Z. Tang, F. Qin, Y. Li, Y. Wang, F. Hao, S. Venkatesan, W. Li, S. Baldelli, A. M. Guloy, H. Fang, Y. Hu, Y. Yao, Z. Wang and J. Bao, *Chem. Mater.*, 2016, **28**, 7385–7393.

27 G. Grancini, V. D'Innocenzo, E. R. Dohner, N. Martino, A. R. Srimath Kandada, E. Mosconi, F. De Angelis, H. I. Karunadasa, E. T. Hoke and A. Petrozza, *Chem. Sci.*, 2015, **6**, 7305–7310.

28 J. S. Manser, M. I. Saidaminov, J. A. Christians, O. M. Bakr and P. V. Kamat, *Acc. Chem. Res.*, 2016, **49**, 330–338.

29 J. Zhao, Y. Deng, H. Wei, X. Zheng, Z. Yu, Y. Shao, J. E. Shield and J. Huang, *Sci. Adv.*, 2017, **3**, eaao5616.

30 F. Huang, Y. Dkhissi, W. Huang, M. Xiao, I. Benesperi, S. Rubanov, Y. Zhu, X. Lin, L. Jiang, Y. Zhou, A. Gray-Weale, J. Etheridge, C. R. McNeill, R. A. Caruso, U. Bach, L. Spiccia and Y.-B. Cheng, *Nano Energy*, 2014, **10**, 10–18.

31 L. Lee, J. Baek, K. S. Park, Y.-E. Lee, N. K. Shrestha and M. M. Sung, *Nat. Commun.*, 2017, **8**, 15882.